The Impact Fracture Behavior of Aluminum Alloy 2024-T351: Influence of Notch Severity

T.S. Srivatsan, Julie Champlin, J. Zakrajsek, P.C. Lam, and M. Manoharan

(Submitted 6 June 1998; in revised form 14 November 2000)

In this paper, the interactive influences of notch severity and test temperature on the impact properties and fracture behavior of a Al-Cu-Mg alloy 2024 in the T351 microstructural condition is presented and discussed. Notch angles of 45, 60, 75, and 90° were chosen for a standard Charpy impact test specimen containing two notches. For a given angle of the notch, an increase in dynamic fracture toughness, with test temperature, is most significant for the least severe of the notches, *i.e.*, 45°. At a given test temperature, the impact toughness decreased with an increase in notch severity. An increase in notch severity resulted in Mode I dominated failure at all test temperatures. The influence of localized mixed-mode loading is minimal for the alloy in the T351 microstructural condition. The impact fracture behavior of the alloy is rationalized in light of alloy microstructure, mechanisms governing fracture, and the deformation field ahead of the propagating crack.

Keywords alloy 2024-T351, aluminum, impact testing, notch severity, temperature

1. Introduction

During the time period spanning the last 3 decades, a wide variety of aluminum alloys, in a spectrum of tempers, have been developed to provide specific combinations of high monotonic strength, ductility, toughness, high-cycle fatigue resistance, and relative ease in fabrication. The relatively high strength-to-weight ratio coupled with low cost and easy availability, in a variety of product forms, makes aluminum alloys an ideal choice for a plethora of engineering applications. The preponderance of carefully orchestrated experimental research work, during the time period starting with the early 1970s and until now, has largely been confined to developing an understanding of intrinsic microstructural influences on mechanical properties such as strength, ductility, fatigue crack initiation resistance, crack growth characteristics, and fracture toughness of aluminum alloys.[1,2] All these studies were confined to essentially Mode I dominated loading condition. However, in many real world situations, several engineering components and civil structures are often subjected to a mixed-mode loading[3–8] and fracture is exacerbated under conditions approaching dynamic loading. This has provided an adequate impetus to understand both the mechanical and fracture behavior of materials when subjected to dynamic loads.

Classical experimental fracture mechanics approaches aimed at quantifying the energy absorption capability of components and/or structures, while concurrently establishing a fundamental understanding of the mechanisms governing the fracture behavior of materials subjected to impact loading, have essentially relied upon impact testing using the Charpy V-notch (abbreviated as CVN) type test specimen. In many practical situations, it is possible to have more than one dominant crack in the material that is under the influence of dynamic loading. Consequently, there exists a need to establish the impact fracture toughness of the aluminum alloys and to concurrently characterize intrinsic microstructural effects on both the macroscopic and microscopic fracture behavior of alloys having more than one macroscopic crack. An attempt to establish the influence of multiple macroscopic cracks on toughness and fracture behavior is important in the evolution of appropriate microstructure and design criteria for structural reliability under impact loading.

The primary objectives of this research are to present details of a study aimed at quantifying the energy absorption capability and to establish the fracture susceptibility of a high-strength Al-Cu-Mg alloy having multiple cracks of varying degrees of severity. Samples of the alloy were subjected to impact loading using the CVN type test specimen.

2. Material and Microstructure

The demand set by the aircraft industry for lightweight, fuel-efficient structures led to the development and emergence of aluminum alloy 2024. The alloy was provided by the Aluminum Company of America (ALCOA, Pittsburgh, PA) as 25 mm thick rolled plate in the T351 temper. The chemical composition (in weight percent) of the alloy is given in Table 1. The presence of magnesium accelerates and intensifies the natural aging response. Iron and silicon are present as the impurity elements. They precipitate as coarse second-phase particles during ingot solidification. The presence of manganese in the alloy is for purposes of grain refinement. It combines with aluminum and copper to form the dispersoid phase (type $Al_{20}Cu_2Mn_3$) that precipitates in abundance during the ingot preheat and high-temperature homogenization treatments.[9] The $Al_2Cu_2Mn_3$ dispersoid particles favor recrystallization and cause the grains

T.S. Srivatsan, Julie Champlin, P.C. Lam, and **J. Zakrajsek,** Department of Mechanical Engineering, The University of Akron, Akron, OH 44325-3903; and **M. Manoharan,** Division of Applied Sciences, Nanyang Technological University, Nanyang Avenue, Singapore 639798. Contact e-mail: tsrivatsan@uakron.edu.

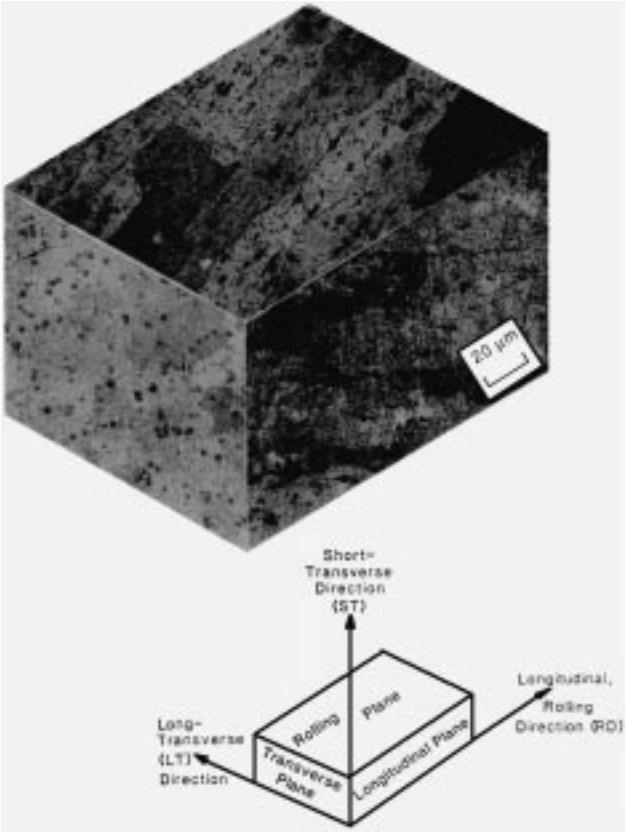

Fig. 1 Triplanar optical micrograph illustrating the microstructure of aluminum alloy 2024-T351 along the three orthogonal directions of the rolled plate

Table 1 Chemical composition of aluminum alloy 2024-T351 (weight percent)

Si	Fe	Cu	Mn(a)	Mg	Al
0.04	0.08	4.42	0.60	1.51	Balance

(a) Present as grain refining element

formed during solution heat treatment to be moderately elongated or flattened.

A triplanar optical micrograph illustrating grain structure of the material in the three orthogonal directions of the wrought plate is as shown in Fig. 1. The as-received 2024-T351 material was fully recrystallized with fairly large recrystallized grains that were both flattened and elongated parallel to the longitudinal direction of the wrought plate, as a direct consequence of mechanical deformation induced by the rolling operation. The insoluble iron-rich and silicon-rich second-phase particles were observed randomly distributed along the three orthogonal directions of the wrought plate. At regular intervals, a clustering or agglomeration of the coarse second-phase particles was evident, resulting in particle-rich and particle-depleted regions. The coarse particles range in size from about 0.5 to 2.0 μm.

Transmission electron microscopy observations of the intrinsic microstructural features revealed the following:

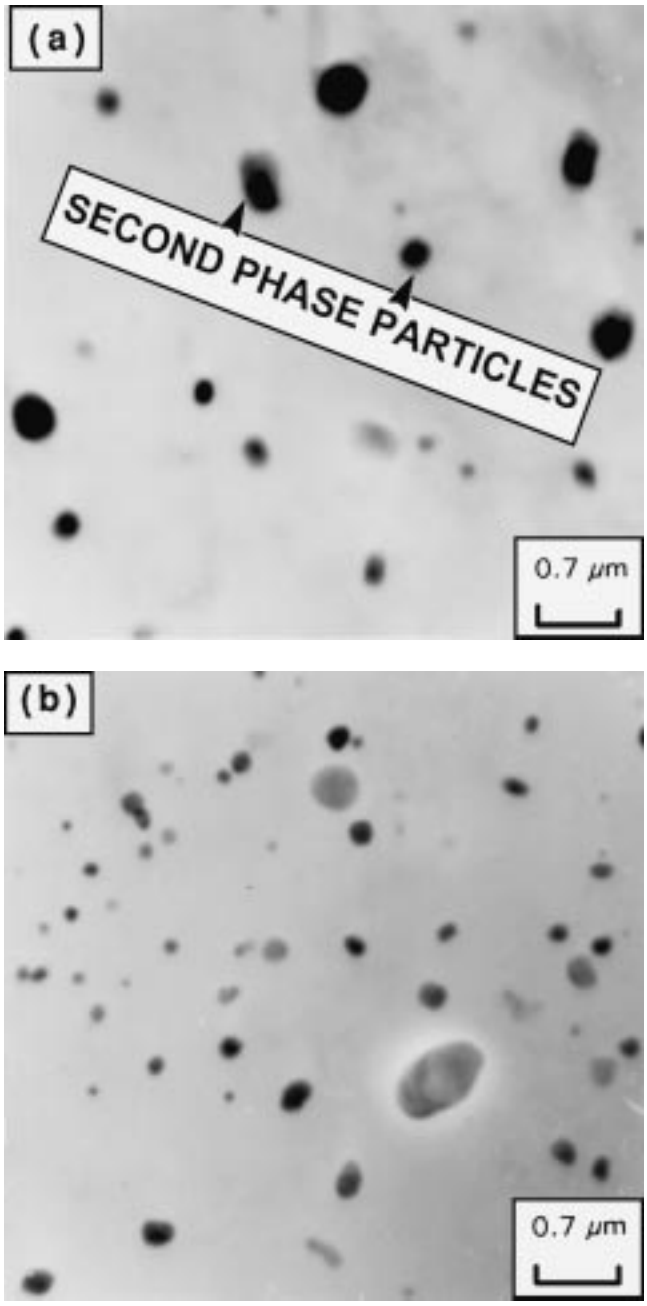

Fig. 2 (**a**) and (**b**) Bright-field transmission electron micrographs showing distribution of the coarse and intermediate size second-phase particles

- a near uniform distribution of the intermediate size dispersoid particles (type $Al_{20}Cu_2Mn_3$) in the alloy matrix (Fig. 2a);
- coarse second-phase particles randomly distributed in the interior (Fig. 2b); the second-phase particles were found both at and along, *i.e.*, "decorating," the grain boundaries (Fig. 3a); and
- an absence of precipitate-free zones (PFZs) both at the high-angle grain boundaries and at the grain boundary triple junctions (Fig. 3b).

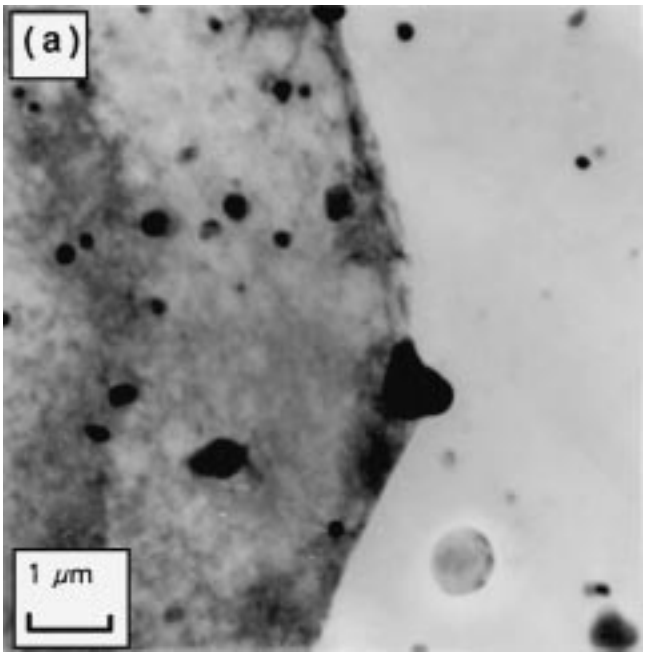

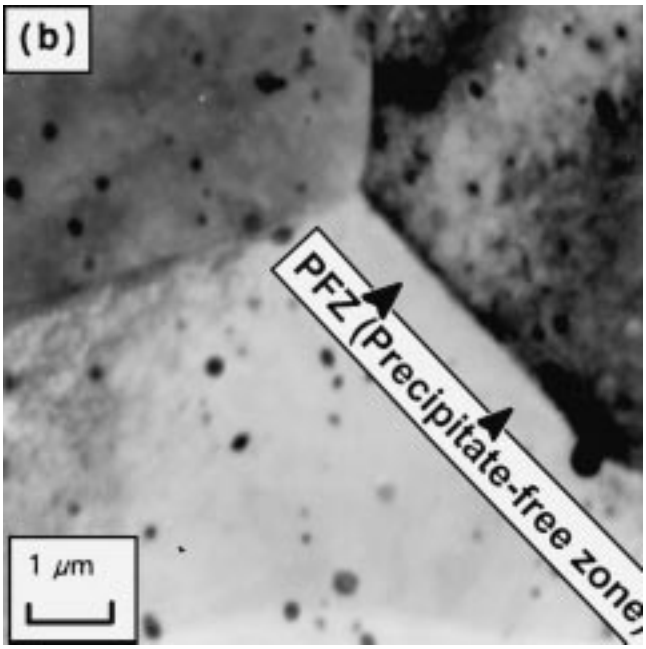

Fig. 3 Bright-field transmission electron micrograph showing (**a**) coarse intermetallic particle pinning of the grain boundary and (**b**) grain boundary triple junction and an absence of PFZ

3. Experimental Techniques

A schematic of the modified Charpy impact test specimen is shown in Fig. 4. The impact test specimens were prepared from the 2024-T351 rolled plate in the "TL" orientation and tested in accordance with specifications outlined in ASTM Standard E-23-93.[10] Crack severity was altered by using different angles of the notch. Four notch angles (defined in this paper as the inclination of the notch face to the flat surface of the test specimen) of 45, 60, 75, and 90° were chosen. For a given notch angle, the orientation of the two cracks in the test specimen was such that they were parallel to each other and at right angles to the applied load. Due to a limited availability of material and test samples, only two tests were performed at the temperatures of (a) liquid nitrogen (−190 °C), (b) dry-ice (−70 °C), (c) ambient temperature (30 °C), and (d) boiling water (100 °C). The specimens were exposed to the temperature (environment) for a full 30 min prior to the initiation of mechanical testing. The modified Charpy impact test specimen provides for a simple method to determine the mutually interactive influences of impact loading, notch severity, and test temperature on dynamic toughness and fracture resistance of a structure having multiple macroscopic cracks.

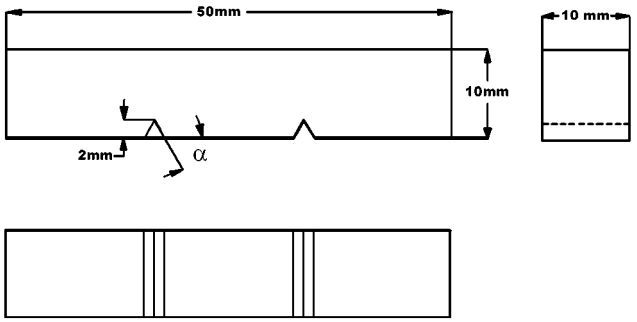

Fig. 4 Schematic of the modified Charpy impact test specimen. The angle ALPHA (α) has values of 45, 60, 75, and 90°

Table 2 Influence of temperature on impact toughness of aluminum alloy 2024-T351(a)

Notch angle (degrees)	Energy absorbed (N m)			
	−190 °C	−70 °C	30 °C	100 °C
45	14	16	16	18
60	12	18	27	26
75	14	18	20	15
90	14	15	18	22

(a) Values are the mean based on duplicate tests

4. Results and Discussion

4.1 Impact Testing Properties

The impact test results summarized in Table 2 are the average values based on duplicate tests. For a given degree of notch severity, that is, 45, 60, 75, and 90° (equivalent to a fine slit), the total energy absorbed during dynamic fracture essentially increased with an increase in test temperature from that of liquid nitrogen (−190 °C) to that of boiling water (100 °C). The increase in energy absorbed to fracture, with test temperature, was significant and noticeable for the alloy samples with the 60° notch and only marginal for the samples having the 45, 75, and 90° notch over the range of test temperatures from cryogenic to elevated. The overall influence of notch severity and test temperature on absorbed energy is exemplified in Fig.

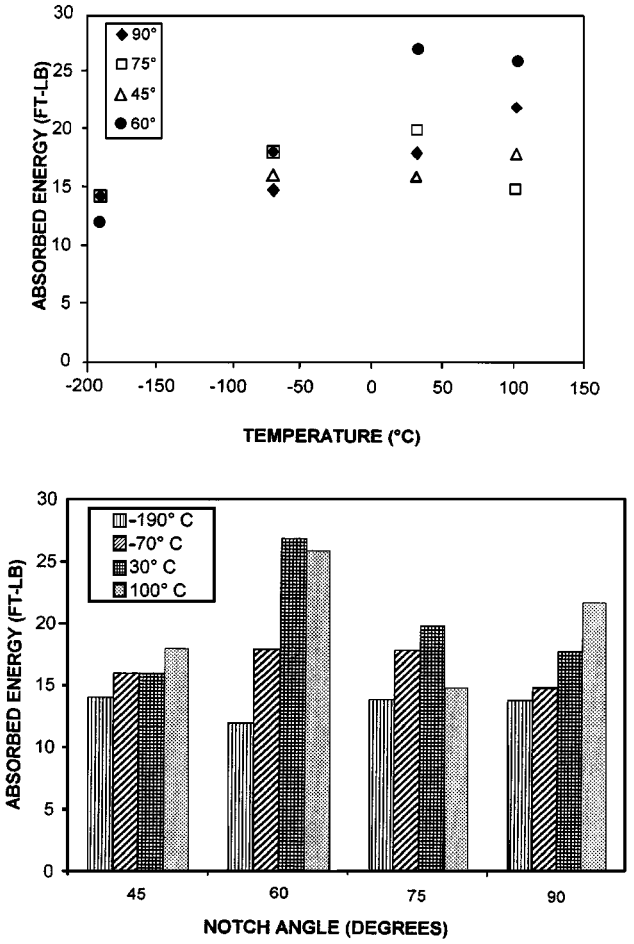

Fig. 5 Schematic showing the variation of absorbed energy with test temperature for different degrees of notch severity

5. The results suggest that for a given notch angle decreasing the test temperature is detrimental to dynamic fracture toughness (absorbed energy in N m) of the CVN specimen for the case of two coplanar cracks. At the lower test temperatures of −190 °C and −70 °C, the impact toughness (absorbed energy in N m) was essentially the same regardless of the degree of notch severity. However, at the test temperatures of 30 °C and 100 °C, the modified CVN specimens with the 60° notch revealed much better impact toughness than those specimens with the 45, 75, and 90° notch angles. The inferior impact toughness of the samples with the 45, 75 , and 90° notch angles is rationalized based on scanning electron microscopy (SEM) observations of the impact fracture surfaces.

4.2 Dynamic Fracture

Representative micrographs of the dynamically deformed impact samples having notch angles of 45, 60, 75, and 90° are shown in Fig. 6 to 12. The scanning electron micrographs support the observations made on the influence of notch severity and test temperature on the energy absorbed to fracture during impact loading. For the alloy samples having the 45° notch and deformed at −190 °C, the fracture surfaces revealed the following features:

- macroscopically brittle failure with an array of macroscopic and fine microscopic cracks randomly distributed through the fracture surface (Fig. 6a); and
- pronounced microscopic cracking arising from fracture of the coarse second-phase particles (Fig. 6b).

In the dry ice temperature (−70 °C), macroscopic cracking was evident along the high-angle grain boundaries coupled with numerous fine microscopic cracks (Fig. 7b) and cracked particles (Fig. 7c), features reminiscent of locally brittle failure mechanisms. Isolated pockets of shallow dimples and randomly distributed voids, features reminiscent of locally ductile mechanisms, were also evident on the fracture surface.

Dynamic fracture of the impact samples with the 60° notch angle was macroscopically brittle and revealed little difference at the temperatures of 30 °C and 100 °C. Figure 8 shows the fracture features of the sample deformed at 30 °C. Overall, fracture was essentially Mode I dominated (Fig. 8a) with the fracture surface covered with a population of fine microscopic cracks of varying size (Fig. 8c). Observations at higher magnifications revealed the following:

- failure of the coarse second-phase particles either by cracking or decohesion at the matrix-particle interfaces; and
- an absence of features reminiscent of locally ductile mechanisms.

The fracture surfaces of the alloy sample deformed at 100 °C was macroscopically brittle and essentially Mode I dominated with limited evidence of localized shear or elongated dimples (Fig. 9a). Microscopically, the fracture surface was covered with numerous fine cracked second-phase particles (Fig. 9b).

The dynamic fracture surface of the alloy sample with 75° notch angle also revealed an overall brittle morphology with Mode I dominated failure at all test temperatures. The fracture surface was covered with (a) a fine population of macroscopic and fine microscopic cracks, (b) cracked second-phase particles, and (c) isolated pockets of voids of varying size. Representative fractographs of the alloy sample dynamically deformed at −70 °C are shown in Fig. 10. Scanning electron microscope observations of the fracture surfaces of the 2024-T351 alloy sample with the 90° notch angle also revealed macroscopically brittle Mode I dominated failure at all test temperatures (Fig. 11 and 12).

As a direct consequence of the large volume fraction of coarse and intermediate size second-phase particles in the microstructure, the occurrence of localized shear and its ability at limiting the Mode I flow field is adversely restricted.[11–15] Overall failure of the T351 microstructure having multiple macroscopic cracks was essentially brittle regardless of the test temperature. Furthermore, regardless of the degree of notch severity, this Al-Cu-Mg alloy in the T351 temper has low to marginal value of dynamic fracture toughness, over the range of test temperatures examined, with no influence of any localized mixed-mode loading on the overall dynamic fracture toughness of the alloy. The marginal increase in the dynamic fracture toughness of the 2024-T351 alloy samples with an increase in test temperature is attributed to the loss of strength and a concomitant enhancement in tensile ductility, with no influence of any localized Mode II component on the overall dynamic toughness.

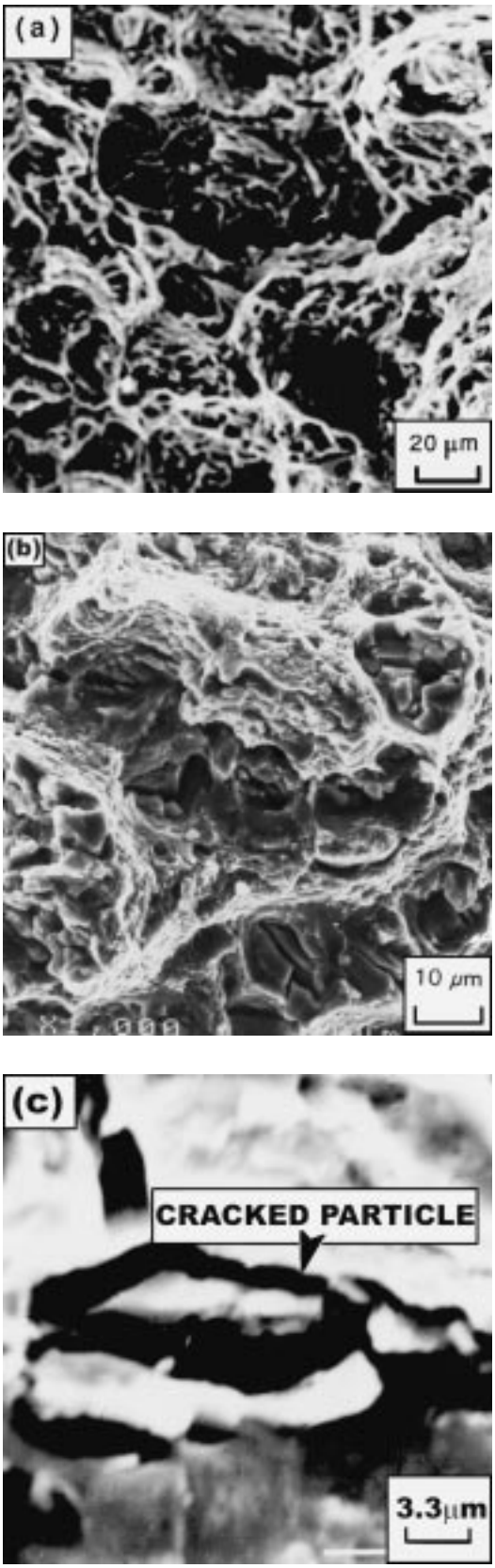

Fig. 6 Scanning electron micrographs of an alloy sample with 45° notch and dynamically deformed at −190 °C showing (**a**) overall morphology, (**b**) microscopic cracking, and (**c**) cracked particle

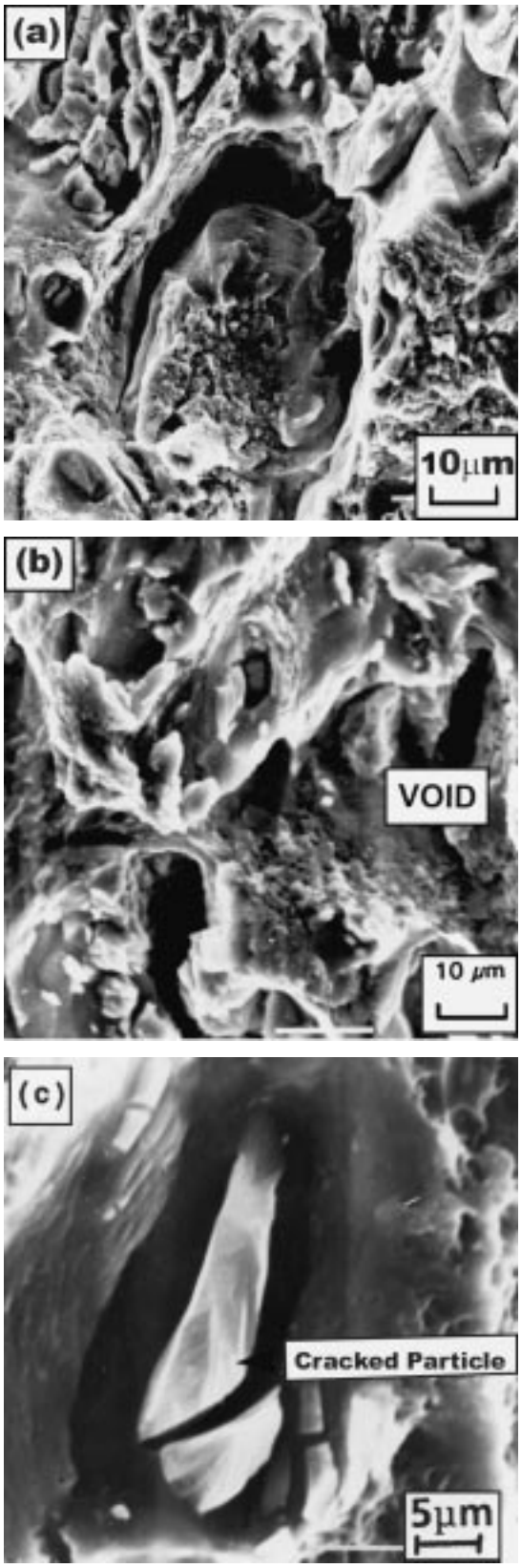

Fig. 7 Scanning electron micrographs of the alloy sample with 45° notch and deformed at −70 °C showing (**a**) overall morphology showing thumb-nail cracking, (**b**) microcracks and isolated macroscopic voids, and (**c**) cracked particles

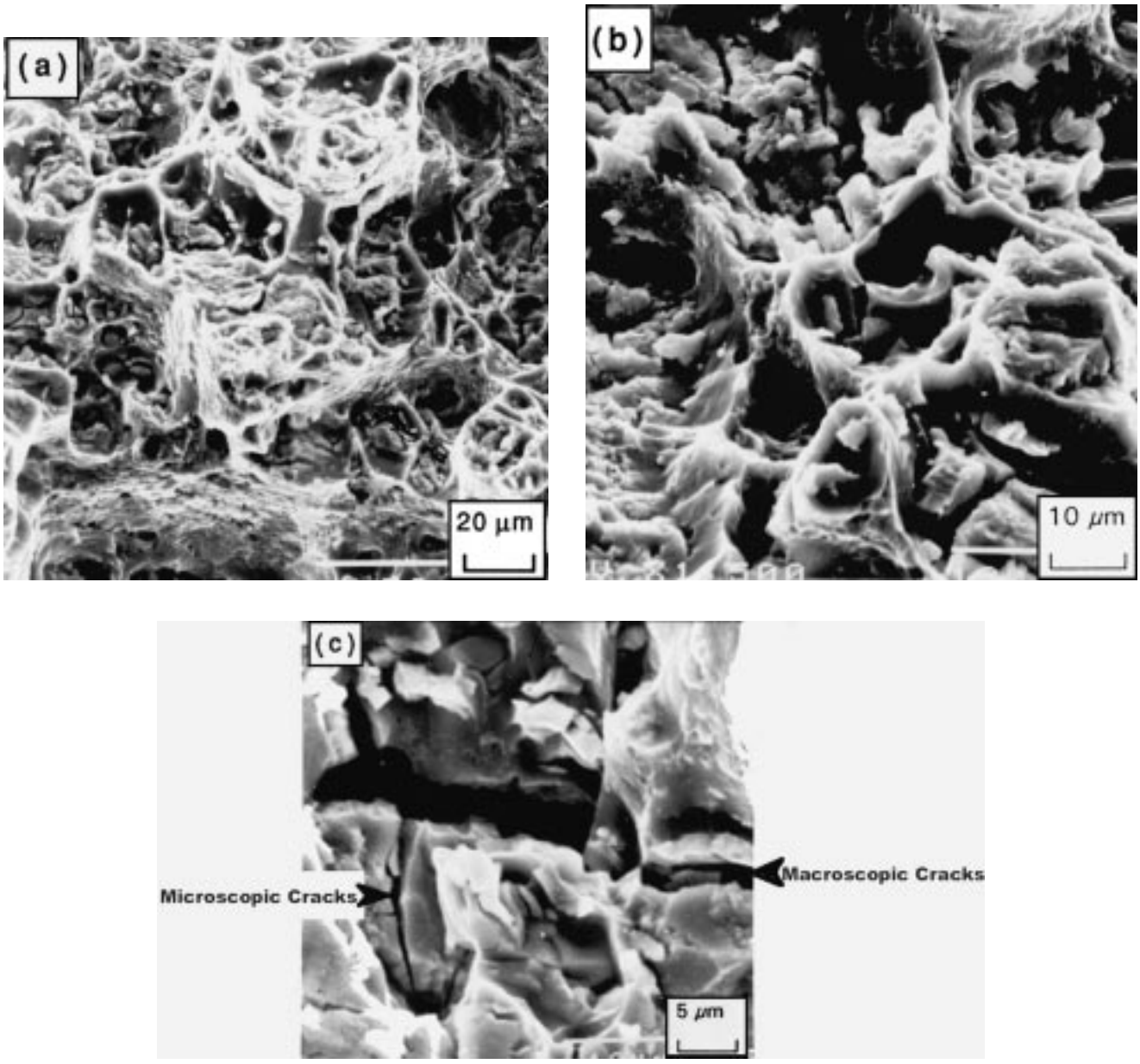

Fig. 8 Scanning electron micrographs of the alloy sample with 60° notch and dynamically deformed at room temperature and showing (**a**) overall morphology, (**b**) voids and shallow dimples, and (**c**) macroscopic and fine microscopic cracks

The presence of a large volume fraction of intrinsically brittle second-phase particles causes them to crack at low values of applied strain. The cracking of the second-phase particles is exacerbated as they fall in the domain of the "process zone" immediately ahead of the rapidly propagating macroscopic crack. The limited formation of fine microscopic voids and shallow dimples suggests the presence of a highly localized Mode II deformation field and its little influence on the dominating Mode I deformation field. Furthermore, because of the dynamic nature of loading and the concomitant rapid propagation of the macroscopic cracks through the microstructure, the overall fracture process is less governed by either the growth and coalescence of the macroscopic and fine microscopic voids or the linkage of the macroscopic voids by the fine secondary void sheets formed around the intermediate size dispersoid particles ($Al_{20}Cu_2Mn_3$). The net result is an absence of shear localization caused by the Mode II deformation field resulting in an essentially Mode I dominated failure. This mechanism is validated by the observation of unstable crack extension in this alloy.

5. Conclusions

In this experimental study on establishing the influence of notch severity on the dynamic response and fracture behavior of aluminum alloy 2024-T351 having two macroscopic cracks, the following key observations are made.

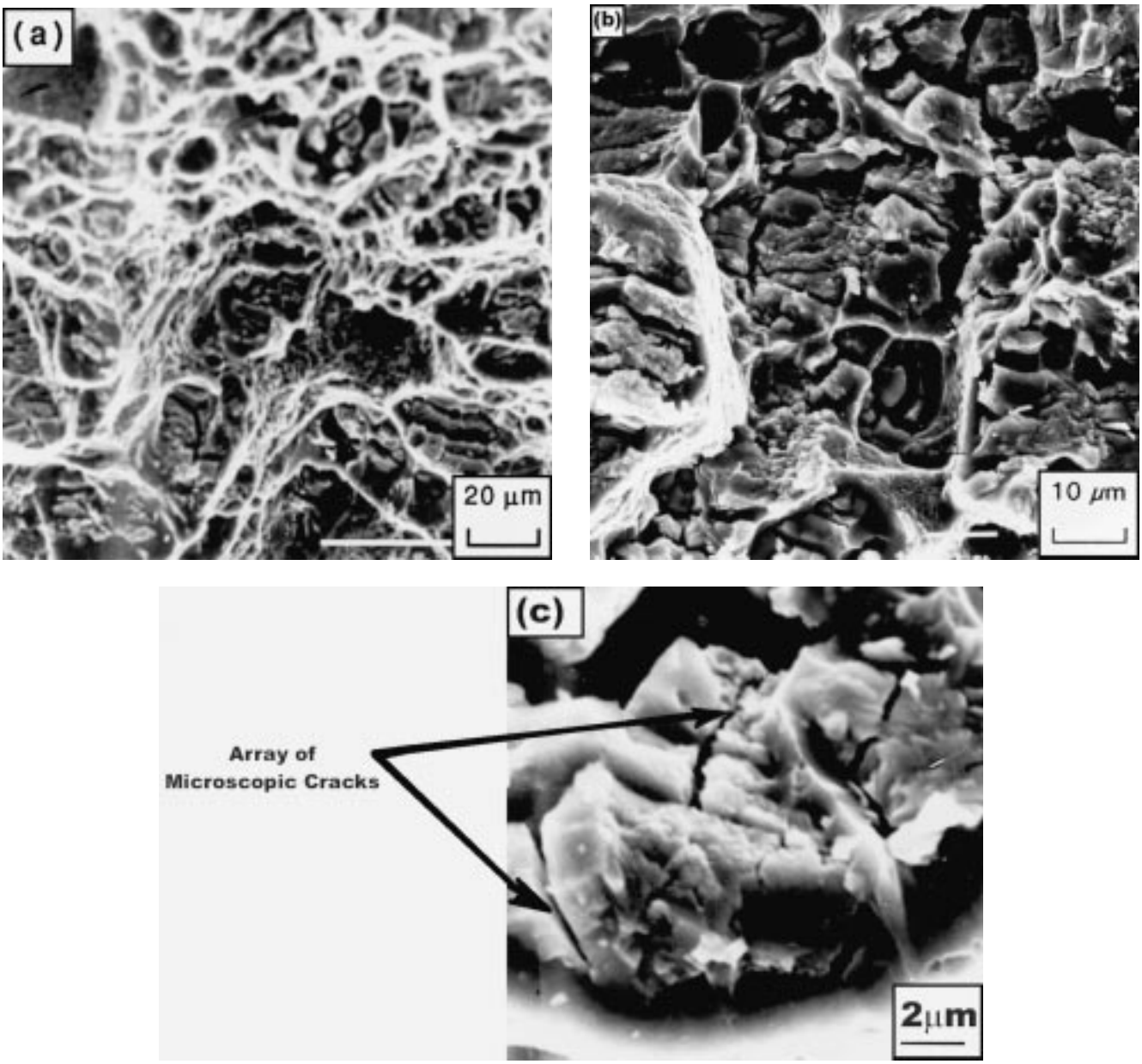

Fig. 9 Scanning electron micrographs of the fracture surface of an alloy sample dynamically deformed at 100 °C, with 60° notch, showing (**a**) overall morphology showing randomly distributed voids and isolated pockets of dimples, (**b**) microscopic cracks and cracked particles, and (**c**) high magnification of (**a**) showing an array of fine microscopic cracks

- The current set of experiments using a modified CVN specimen suggest that, for the very ductile temper (T351) of alloy 2024 and for a given notch geometry, the dynamic fracture toughness increases with an increase in test temperature.
- At a given test temperature, the notch toughness of alloy 2024-T351 decreases with an increase in notch severity.
- For the least severe of the notches, *i.e.*, notch angle of 60°, the increase in dynamic fracture toughness with temperature was most appreciable.
- Macroscopic fracture mode and microscopic fracture features failed to provide convincing evidence of the occurrence of localized mixed-mode loading at the higher test temperatures.
- With an increase in notch severity, fracture surface appearance revealed essentially Mode I dominated failure at all temperatures with features reminiscent of locally brittle failure.

Acknowledgments

This research effort was jointly supported by The University of Akron (Akron, OH), The State of Ohio: Board of Regents (Columbus, OH), with material support from the Aluminum Company of America (Pittsburgh, PA).

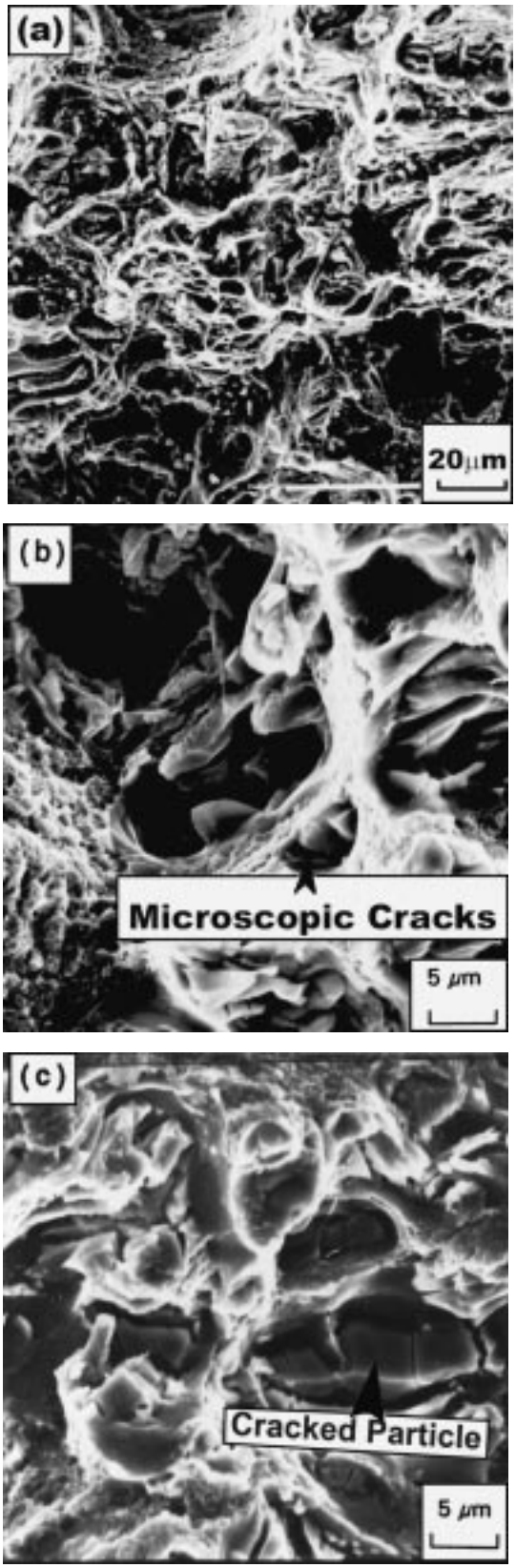

Fig. 10 Scanning electron micrographs of the fracture surface of the dynamically deformed sample with 75° notch showing (**a**) overall morphology, (**b**) macroscopic and microscopic cracking, and (**c**) cracked particles and macroscopic voids

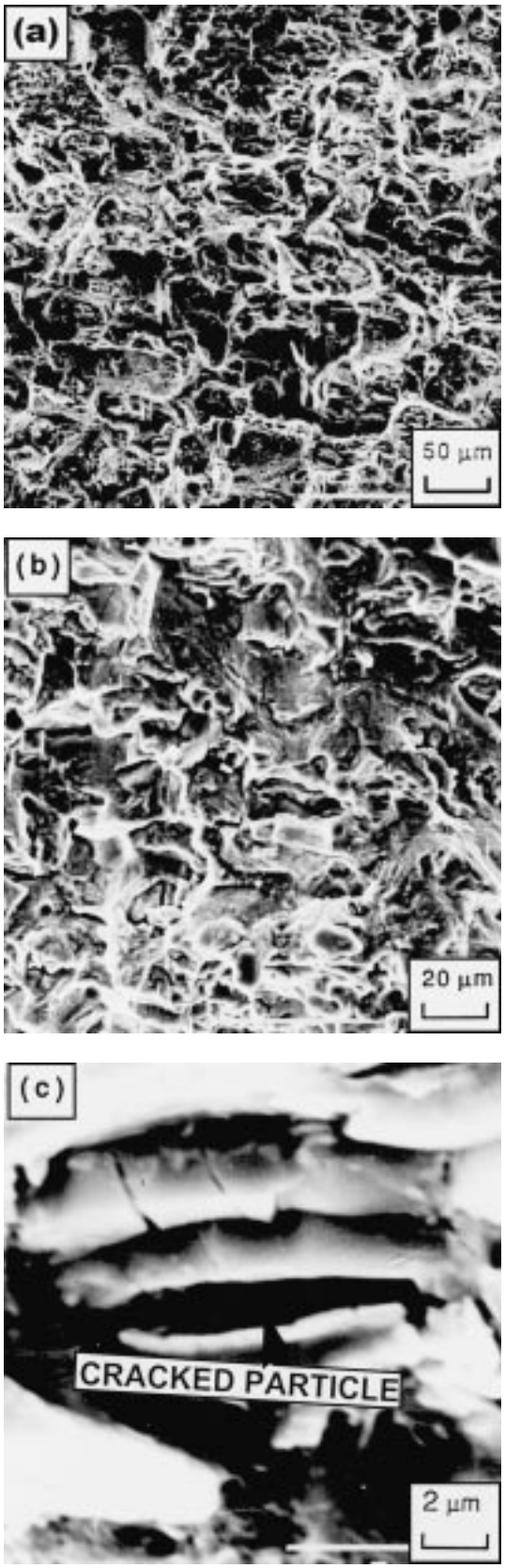

Fig. 11 Scanning electron micrographs of a sample with notch angle of 90° and dynamically deformed at −190 °C, showing (**a**) overall morphology, (**b**) high magnification of (**a**), and (**c**) cracked particles

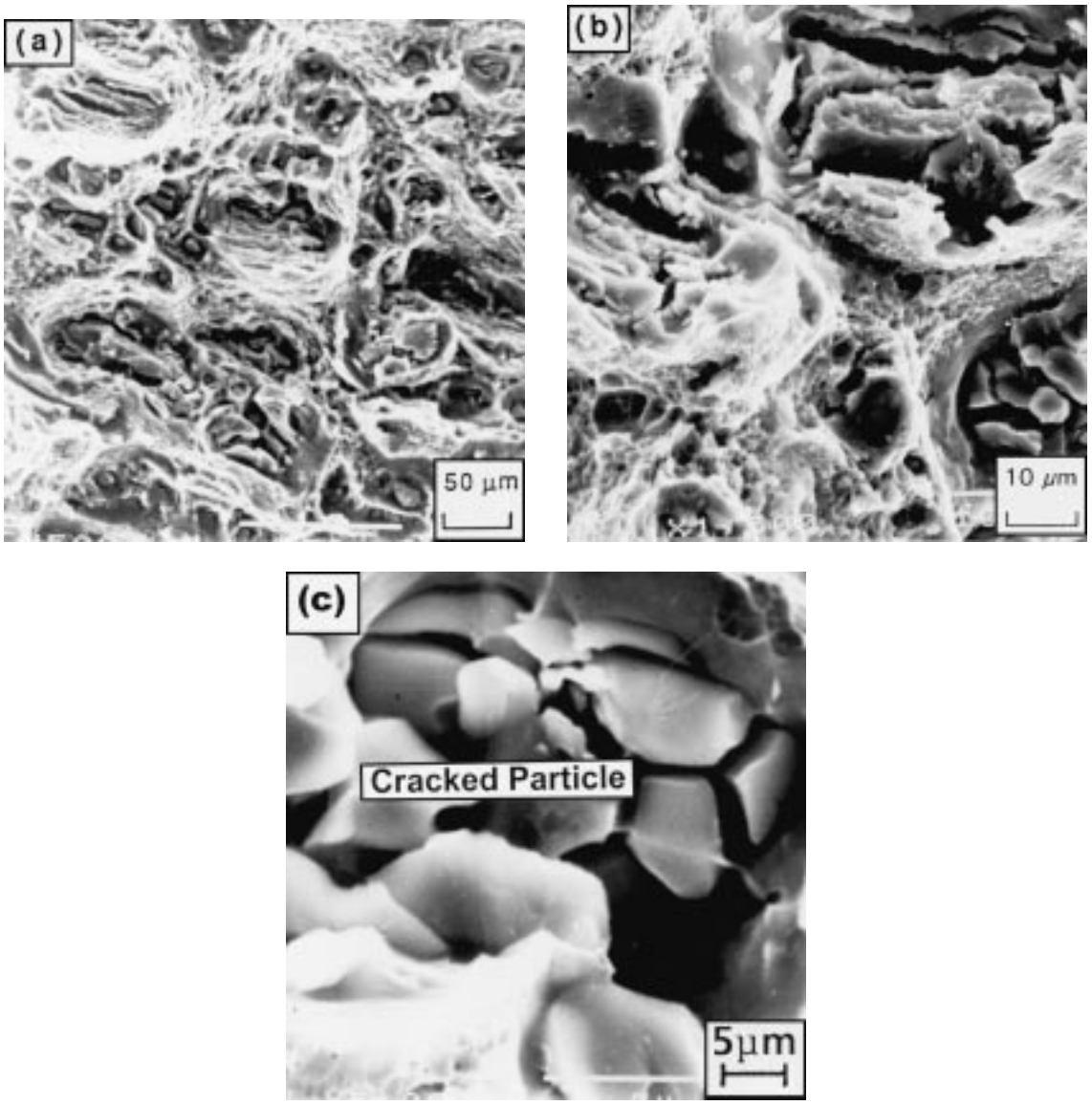

Fig. 12 Scanning electron micrographs of a sample with notch angle of 90° and dynamically deformed at 100 °C, showing (**a**) overall morphology, (**b**) high magnification of (**a**): macroscopic and fine microscopic cracks, and (**c**) cracked intermetallic particle

References

1. M. Yoda: *Eng. Fract. Mech.*, 1980, vol. 13, p. 647.
2. R.J. Bucci: *Eng. Fract. Mech.*, 1979, vol. 12, pp. 407-41.
3. Y. Ueda, K. Ikeda, T. Yao, and M. Aoki: *Eng. Fract. Mech.*, 1983, vol. 18, p. 1131.
4. M.T. Miglin, J.P. Hirth, and A.R. Rosenfield: *Int. J. Fract.*, 1983, vol. 22, p. R65.
5. M.T. Miglin, J.P. Hirth, and A.R. Rosenfield: *Res. Mechanica*, 1984, vol. 11, p. 85.
6. J.G. Schroth, J.P. Hirth, R.G. Hoagland, and A.R. Rosenfield: *Metall. Trans. A*, 1987, vol. 18A, p. 1061.
7. M. Manoharan, J.P. Hirth, and A.R. Rosenfield: *Scripta Metall.*, 1989, vol. 23, p. 763.
8. S.V. Kamat, J.P. Hirth, and R. Mehrabian: *Scripta Metall.*, 1989, vol. 23, p. 523.
9. E.A. Starke, Jr.: *Mater. Sci. Eng.*, 1977, vol. 29, pp. 99-115.
10. ASTM Standard E-23-93: "Standard Method for Notched Bar Impact Testing of Metallic Materials," ASTM, Philadelphia, PA, 1993.
11. V. Tvergaard: *J. Mech. Phys. Solids*, 1987, vol. 35, p. 43.
12. M. Manoharan, S. Raghavachary, J.P. Hirth, and A.R. Rosenfield: *J. Eng. Mater. Technol.*, 1989, vol. 111, p. 440.
13. Manoharan, J.P. Hirth, and A.R. Rosenfield: *J. Testing Eval.*, 1990, vol. 18, p. 106.
14. M. Manoharan, J.P. Hirth, and A.R. Rosenfield: *Acta Metall. Mater.*, 1991, vol. 39, p. 1203.
15. A.M. Kumar and J.P. Hirth: *Scripta Metall. Mater.*, 1991, vol. 25, p. 981.